molecular pharmaceutics

pubs.acs.org/molecularpharmaceutics

Article

Comparison of Amorphous Solid Dispersions of Spironolactone Prepared by Spray Drying and Electrospinning: The Influence of the Preparation Method on the Dissolution Properties

Edina Szabó, Petra Záhonyi, Dániel Brecska, Dorián L. Galata, Lilla A. Mészáros, Lajos Madarász, Kristóf Csorba, Panna Vass, Edit Hirsch, Joanna Szafraniec-Szczęsny, István Csontos, Attila Farkas, Guy Van denMooter,* Zsombor K. Nagy,* and György Marosi

Cite This: *Mol. Pharmaceutics* 2021, 18, 317−327

Read Online

ACCESS | Metrics & More | Article Recommendations

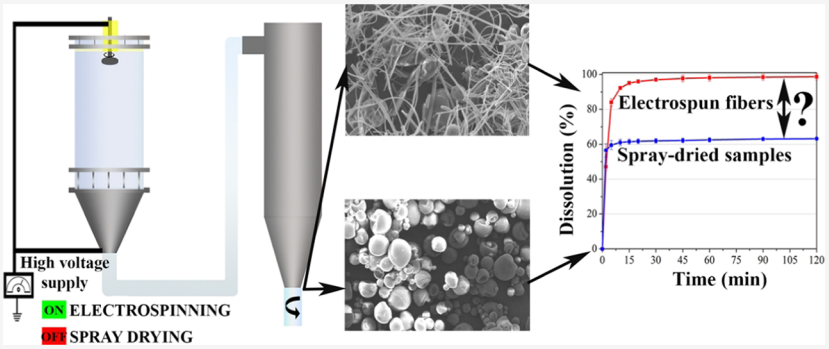

ABSTRACT: This research aimed to compare two solvent-based methods for the preparation of amorphous solid dispersions (ASDs) made up of poorly soluble spironolactone and poly(vinylpyrrolidone-*co*-vinyl acetate). The same apparatus was used to produce, in continuous mode, drug-loaded electrospun (ES) and spray-dried (SD) materials from dichloromethane and ethanol-containing solutions. The main differences between the two preparation methods were the concentration of the solution and application of high voltage. During electrospinning, a solution with a higher concentration and high voltage was used to form a fibrous product. In contrast, a dilute solution and no electrostatic force were applied during spray drying. Both ASD products showed an amorphous structure according to differential scanning calorimetry and X-ray powder diffraction results. However, the dissolution of the SD sample was not complete, while the ES sample exhibited close to 100% dissolution. The polarized microscopy images and Raman microscopy mapping of the samples highlighted that the SD particles contained crystalline traces, which can initiate precipitation during dissolution. Investigation of the dissolution media with a borescope made the precipitated particles visible while Raman spectroscopy measurements confirmed the appearance of the crystalline active pharmaceutical ingredient. To explain the micro-morphological differences, the shape and size of the prepared samples, the evaporation rate of residual solvents, and the influence of the electrostatic field during the preparation of ASDs had to be considered. This study demonstrated that the investigated factors have a great influence on the dissolution of the ASDs. Consequently, it is worth focusing on the selection of the appropriate ASD preparation method to avoid the deterioration of dissolution properties due to the presence of crystalline traces.

KEYWORDS: *amorphous solid dispersion, spray drying, electrospinning, scale-up, dissolution*

1. INTRODUCTION

The number of effective drug candidates is increasing year by year with the advancement of drug discovery strategies such as high throughput screening, combinatorial chemistry, or the application machine learning.[1−3] However, the majority of the promising active pharmaceutical ingredients (APIs) are characterized by poor water solubility,[4] which results in several difficulties during the formulation of oral solid dosage forms. Different formulation strategies are available to enhance the dissolution properties without modifying the structure of the poorly water-soluble drugs[5,6] One of the most common physical modifications is the formulation of amorphous solid dispersions (ASDs).[7] Molecularly dispersed APIs in the polymer matrices

Received: September 25, 2020
Revised: November 22, 2020
Accepted: November 24, 2020
Published: December 10, 2020

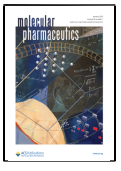

result in higher dissolution; therefore, increasing the bioavailability of the drug.

Numerous technologies have been developed during the last few decades for the preparation of ASDs with high productivity and efficiency. As a result, more and more ASD-loaded products have entered the pharmaceutical market, which proves the feasibility of this formulation strategy.[8] In general, ASD preparation methods are classified into three groups, namely the solvent-based methods, the melt (or fusion) methods, and mechanochemical activation (e.g., ball milling) methods.[9] The preparation method can influence the dissolution,[10−12] the bioavailability,[13] the downstream processing,[14] and the stability of the ASDs.[15,16] Furthermore, the properties of the APIs can also determine the applied downstream methods and used excipients.[17−19]

Half of the FDA-approved ASD-loaded products are prepared by the solvent-based methods,[8] which is a particularly good choice in the case of thermosensitive APIs. The majority of the marketed products are prepared by spray drying since it is a simple and effective technique for preparing ASDs.[20,21] Although the application of temperatures above the melting points is not needed, the removal of residual solvents is a huge challenge in solvent-based techniques. On the one hand, there are strict quality requirements related to the limit of the residual solvents, especially the organic solvents.[22] On the other hand, the moisture uptake of some hydrophilic polymers decreases the glass transition temperature, which has a high correlation with the deterioration of dissolution properties and stability.[23−25] In this context, different drying kinetics can be observed for various solvent methods, and thus the quality and the main properties of the products are also distinct.[26−28] In the case of certain drug−polymer solutions and methods, the solvent evaporation rate is not fast enough, and thus ASDs with a nonideal structure are formed.[29] Consequently, phase separation and crystallization start,[30] which may lead to a decrease in the dissolution.[31] To handle these problems, several novel techniques have been developed during the last decades such as electrospinning, electroblowing, and electrospraying.[32−38] Besides, electrostatic force-based methods usually require less solvent, highly viscous solutions, and allow very gentle and fast solvent evaporation. Compared to the commonly used spray drying, electrostatic force-based techniques proved to be a more reliable method in many cases to avoid phase separation in ASDs.[27,31,39]

Spironolactone (SPIR) is a suitable model drug used to compare high-productivity technologies of electrospinning and spray drying. SPIR is an antihypertensive and diuretic API with poor water solubility, and it is a widely used model drug in ASDs. Several research papers have been published about successful dissolution enhancement of SPIR via solvent-based or melt methods.[40−43] SPIR possesses five hydrogen-bond acceptor groups, and the application of polymers containing hydrogen-bond donor groups may result in drug−polymer interactions in the ASD, leading to improved physical stability.[44,45] Consequently, the influence of the polymer type on the dissolution of SPIR needs to be considered.[46,47]

This work aimed to compare two different solvent-based methods thus a noninteracting system was chosen to eliminate complex interactions caused by hydrogen-bonding. For this purpose, poly(vinylpyrrolidone-*co*-vinyl acetate) (PVPVA64) was used as a polymer matrix, which has only hydrogen-bond acceptor groups similar to the SPIR (Figure 1). This model system makes it possible to evaluate the effects of the particle shape, the drying rate, and the electrostatic field. To the best of our knowledge, the comparison of spray drying and electrospinning under similar processing conditions and using the same apparatus has not yet been performed. It was expected that such a comparison would highlight the relevance of the preparation method selection, aiming to satisfy the physical stability requirements related to ASDs.

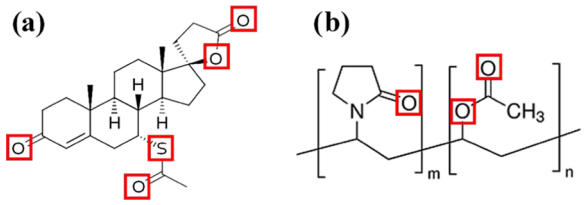

Figure 1. Chemical Structures of SPIR (a) and PVPVA64 (b). Red frames depict the hydrogen-bond acceptor parts of the molecules.

2. MATERIALS AND METHODS

2.1. Materials. Micronized SPIR (Form II) (Figure 1a) (melting point: 211 °C) was received from Gedeon Richter Plc. (Budapest, Hungary). PVPVA64 (Kollidon VA64) (Figure 1b) was kindly provided by BASF (Ludwigshafen, Germany). Dichloromethane (DCM) and absolute ethanol (EtOH) were analytical grade, and both were purchased from Merck Ltd. (Budapest, Hungary) and used without any further purification. For the dissolution tests, 37 w/w % HCl was ordered from Merck Ltd. (Budapest, Hungary).

2.2. Sample Preparation. A multifunctional apparatus was used to prepare SPIR-loaded ASDs (Figure 2) to reduce technological differences.[48,49] The equipment was originally developed for electrospinning, but it can be perfectly operated as a rotary spray dryer. The key element of the machine is a round-shaped, stainless steel spinneret with orifices ($d_{spinneret}$ = 34 mm, $d_{orifice}$ = 330 μm), connected to a high-speed motor. The rotational speed of the spinneret was set to 40 000 rpm during both experiments. ASDs were prepared at ambient temperature (25 °C) and 45 ± 5% relative humidity. A grounded stainless steel cone at the bottom of the drying chamber was used. The products were periodically removed from the grounded metal cone with automated air knives (pressurized blowing air) and were collected in a cyclone, which enabled the application of the system in continuous manufacturing mode. A previously determined drug−polymer ratio was used for electrospinning with 40% SPIR and 60% PVPVA64.[50] The solvent mixture consisted of dichloromethane and ethanol, which were already tested for high-speed electrospinning of itraconazole.[48] During spray drying, a less viscous solution was used than that in the case of electrospinning experiments. Table 1 summarizes the exact amount of raw materials used and the sample codes. The solutions were fed into the spinneret with a Watson−Marlow peristaltic pump (Watson−Marlow Fluid Technology Group, Budapest, Hungary). The applied feeding rates were 300 and 600 mL/h in the case of the electrospinning and spray drying, respectively. For fiber formation, 40 kV positive, a direct current voltage was applied to the grounded stainless steel spinneret during electrospinning. The electrospun (ES) product was pushed through a sieve with a hole size of 0.8 mm after the preparation to achieve a more uniform macroscopic particle size.

The influence of the drying kinetics was also examined through the preparation of samples by film casting. The solution of SPIR and PVPVA64 was cast into square-shaped silicon molds (3 × 50 × 50 mm^3) and dried for 3 days at room

https://dx.doi.org/10.1021/acs.molpharmaceut.0c00965
Mol. Pharmaceutics 2021, 18, 317−327

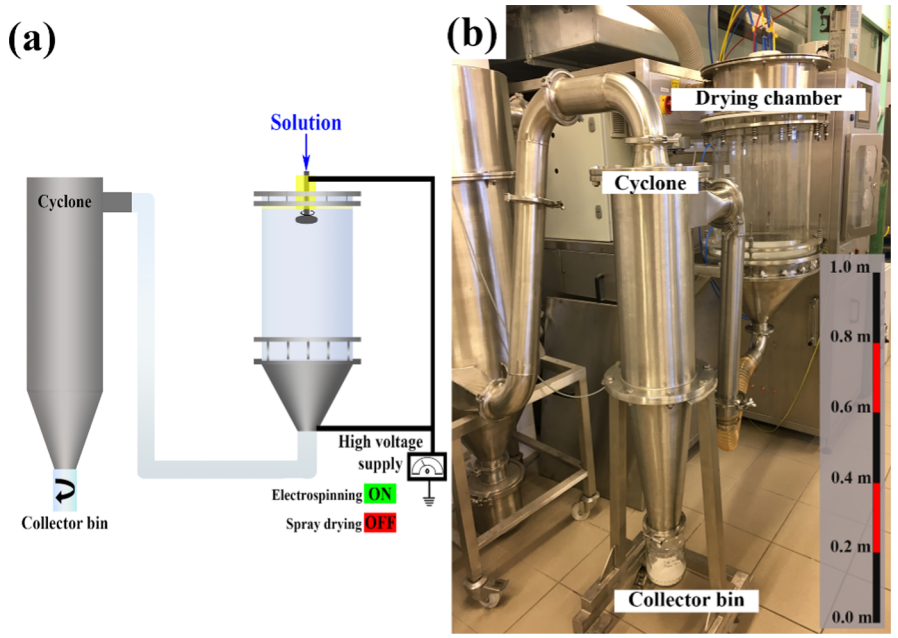

Figure 2. Schematic illustration (a) and photo (b) of the applied multifunctional apparatus.

Table 1. Applied Compositions for Sample Preparation

		SPIR		PVPVA64		DCM/EtOH		productivity
sample code	preparation method	(w/w %)	(g)	(w/w %)	(g)	volume ratio	total volume (mL)	(g/h)
SD	spray drying	40	12	60	18	2:1	160	~70
ES	electrospinning	40	12	60	18	2:1	80	~74
FC	film casting	40	1.2	60	1.8	2:1	8	n.a.
ESY	electrospraying	40	12	60	18	2:1	160	n.a.

temperature. The thickness of the film was 70 ± 5 μm, which was determined with a Pro-Max Electronic Digital Caliper (NSK, Tokyo, Japan). The film was ground into small pieces before the dissolution test with the same sieve, which was used for the ES sample. The composition and the applied abbreviation of the film cast sample can be found in Table 1.

Finally, electrospraying was performed to investigate the effect of the electrostatic field on the quality of the product. Because we planned to achieve a similar round-shaped morphology as in the case of spray drying, the same composition was used (Table 1). The abovementioned multifunctional apparatus was used for the preparation of electrosprayed (ESY) samples. The adjusted process parameters were similar to those applied for spray drying. The only difference was the utilization of 40 kV voltage on the atomizer.

2.3. X-ray Powder Diffraction (XRPD). One of the applied methods for the investigation of the amorphous characteristics of the samples was X-ray powder diffraction. The measurements were performed with a PANalytical X'pert Pro MPD X-ray diffractometer (Almelo, The Netherlands) using Cu Kα radiation (1.506 Å) and a Ni filter. The applied current was 30 mA, while the voltage was 40 kV. The adjusted scan range was between 2θ angles of 4 and 44°.

2.4. Differential Scanning Calorimetry (DSC). The amorphous characteristic of the prepared samples was also examined by DSC. The thermograms were recorded using a Setaram DSC 92 (Caluire, France). Nitrogen flush was introduced into the chamber with a continuous flow of 50 mL/min. The applied temperature program started with an isothermal part of 1 min at ambient temperature, which was followed by linear heating from 25 to 250 °C at a rate of 10 °C/min.

2.5. Thermogravimetric Analysis (TGA) and Mass Loss Measurement. Thermogravimetric analysis of the samples was performed by a Q5000 TGA instrument (TA Instruments). The ES fibers and spray-dried (SD) powder (ca. 10 mg) were heated from 25 to 250 °C at 10 °C/min using a 25 mL/min nitrogen flush.

Solvent evaporation was investigated by a simple mass loss analysis, where the mass of the products was measured over time under atmospheric circumstances (no inert gas was applied). The samples were placed on an analytical balance (Sartorius AC 210 and SQP-F, Göttingen, Germany) at 25 °C for 90 min immediately after preparation. A computer using data processing software (written by the authors) recorded the measured weights.

2.6. Scanning Electron Microscopy (SEM). The morphology and size of the prepared samples were investigated by a JEOL JSM 6380LA (JEOL, Tokyo, Japan) type scanning electron microscope. The specimens were fixed with conductive double-sided carbon adhesive tape. The samples were sputtered with gold before the measurements to avoid electrostatic charging. The SEM examinations were performed in a high vacuum while the applied accelerating voltage and the working distance were 10 kV and between 10 and 15 mm, respectively. A randomized diameter determination method was used to

https://dx.doi.org/10.1021/acs.molpharmaceut.0c00965
Mol. Pharmaceutics 2021, 18, 317−327

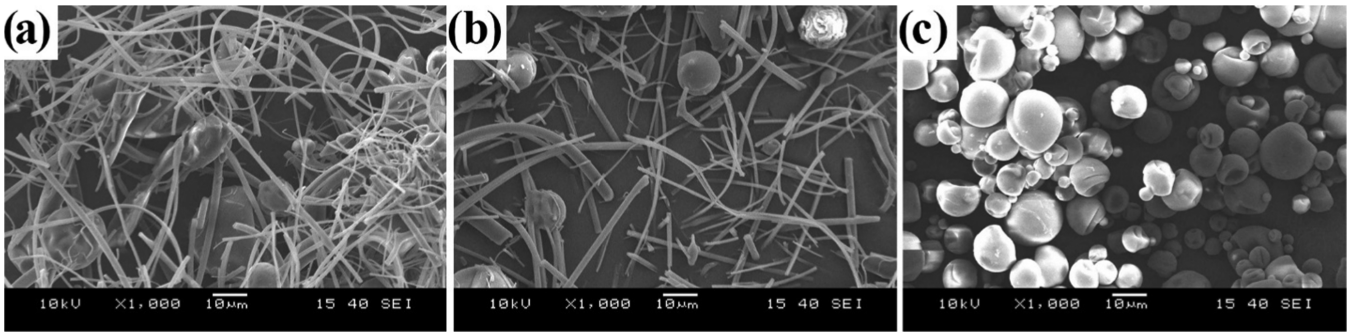

Figure 3. SEM images of the ES before grinding (a), after grinding (b), and the SD (c) samples.

calculate the average diameter of the SD particles and the fibers.[51]

2.7. In Vitro Dissolution Testing. Dissolution of the SPIR-loaded samples was measured with a Pharma Test PTWS 600 dissolution tester (Pharma Test Apparatebau AG, Hainburg, Germany), which was coupled with an Agilent 8453 ultraviolet−visible (UV−vis) spectrophotometer (Agilent Technologies, Santa Clara, CA) for online determination of the dissolved API through a flow cell system. The current concentration of the dissolved SPIR was calculated in real-time based on a preliminarily built calibration at a wavelength of 243 nm. All of the samples were investigated by the so-called "tapped basket" dissolution method, which is a mixture of the basket (USP I) and the paddle (USP II) apparatus.[48] The ES product was pushed through a sieve before the dissolution test. The stirrer speed was set to 50 rpm, and 900 mL of 0.1 N HCl dissolution media at a temperature of (37 ± 0.5) °C was applied during the measurements. The API content was 50 mg in all dissolution tests, and each sample was examined in triplicate.

2.8. Laser Diffraction. The particle size distribution of the ground ES, the SD, and the crushed film-cast (FC) samples were determined by a Malvern Mastersizer 2000 type laser diffractometer (Malvern Instruments Ltd., Worchestershire, U.K.). The background recording took 45 s while the measurement time was set to 1 min. The intensity of the vibrational sample feeder was adjusted to 75%. The applied pressure was 1.5 bar during all measurements. The volume equivalent sphere diameter was used to characterize the particle size. The measured $d_{(0.5)}$ values described the 50% cumulative undersize of the volumetric distribution.

2.9. Polarized Light Optical Microscopy. An Amplival Carl Zeiss (Jena, Germany) polarized microscope with an OLYMPUS C4040 Z type camera was used for the detection of crystalline traces in the prepared samples. The agglomerates of the prepared samples were separated to individual particles with silicon oil during sample preparation. The collection and evaluation of the images were implemented with DP-Soft software.

2.10. Raman Spectroscopy and Mapping. The temperature-induced decomposition of the samples, the effect of the dissolution media on the samples, and the possible crystalline traces in the prepared ASDs were examined with a Horiba Jobin Yvon LabRAM system coupled with an external 785 nm diode laser source and an Olympus BX-40 optical microscope. To increase the confocal performance and reduce the analysis volume, a confocal hole of 500 μm, half of the maximum diameter, was used in the confocal system. In addition, a 950 groove/mm grating monochromator was used to disperse the Raman photons before they reach the CCD detector.

An objective of 20× magnification (laser spot size: ∼3 μm) was applied during the investigation of temperature-induced decomposition and the impact of the dissolution media. The spectrograph position was set to 1200 cm^{-1} to measure the spectral range of 570−1765 cm^{-1} with 4 cm^{-1} resolution. The applied acquisition time was adjusted to 60 s with 2-time accumulation. To examine the temperature-induced decomposition, the temperature of the ES and SD samples were controlled by a Linkam THMS600 heating/cooling stage (Linkam, United Kingdom). The adjusted temperature program comprised linear heating from 25 to 250 °C with a 10 °C/min heating rate. To measure the impact of the HCl solution, pastilles were formed from 100 mg of SD powder and 100 mg of the ES sample, and then 20 μL of the dissolution medium was dropped onto the surface of each pastille. The flat round pastilles were prepared with a Camilla OL95 type press using 50 bar pressure. The thickness and diameter of the pastilles were ∼1.5 and 12 mm, respectively.

Investigation of the crystalline traces in the pure ES and SD samples was performed by Raman mapping, where pastilles of the ASDs were examined. A 50× objective (laser spot size: ∼2 μm) was used for this purpose. The spectral range was the same as in the case of simple spectrum collection. The maps were recorded with a 5 μm step size in both directions and contained 41 × 41 points. Every single spectrum acquisition took 20 s, and two spectra were averaged at each measured point. The evaluation of the Raman mapping was conducted using the classical least-squares (CLS) method in LabSpec 5.41 (Horiba Jobin Yvon S.A.S., Villeneuve d'Ascq, France). Spectra of crystalline SPIR, amorphous SPIR, and PVPVA64 were applied as references during chemometric analysis.

2.11. Borescope. An Olympus A50372A borescope was utilized to investigate the precipitation in the dissolution media. The outer diameter was 5 mm, while the direction of the view was 0°.

3. RESULTS AND DISCUSSION

The main goal of this work was to compare two different solvent-based ASD preparation methods with similar productivity. The effect of the differences in the production circumstances and drying kinetics on the product properties, such as morphology, amorphous characteristics, and dissolution, were investigated. Our aim was to prepare good quality products and make the methods comparable as much as possible. For this reason, the same apparatus with the same collection method, the same solid production rate, the same drying temperature, the same spinneret, and the same rotational speed of the spinneret was used. Overall, there were only three differences between the two methods: the solution concentrations, the adjusted feeding rate

https://dx.doi.org/10.1021/acs.molpharmaceut.0c00965
Mol. Pharmaceutics 2021, 18, 317−327

of the solutions, and the application of high voltage during electrospinning.

3.1. Preparation of the ES and SD Samples. For preparing SPIR-loaded fibers with a small fiber diameter, the feeding rate during the electrospinning experiment was set based on our previous studies. According to the SEM images, fibrous samples were produced successfully with an average fiber diameter of 1.27 ± 0.59 μm (Figure 3a). The fibrous structure was retained even after grinding; therefore, the prepared ASD was found to be suitable for further downstream processing such as blending and tableting (Figure 3b). The particle size analysis of the ground ES samples based on laser diffraction showed multimodal distribution with a $d_{(0.5)}$ = 10.533 μm (Figure 4).

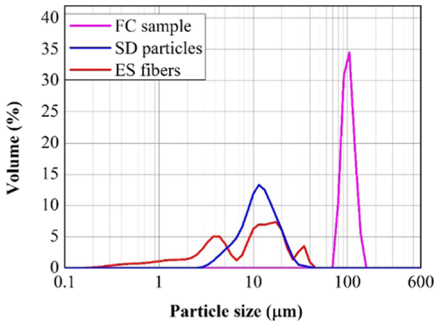

Figure 4. Particle size analysis of ES fibers, SD particles, and the film-cast (FC) sample by laser diffraction.

Multiple peaks were explained by the difference in the size of the agglomerates, which were formed after grinding.[52] A yield of 70% was obtained during fiber preparation, and corresponded to ~70 g/h productivity. This value was much higher than the ~0.01 to 1 g/h productivities, which were achieved by the basic electrospinning setups.[53] In addition, it was possible to enhance the output by increasing the number of spinnerets.[48]

The next step was to achieve similar productivity with spray drying. Twice as much solvent was used to obtain uniform particles with satisfactory efficiency. To achieve ~70 g/h productivity from the lower viscosity solution, a 600 mL/h feeding rate was needed. Since the concentration was half of that used during electrospinning, the doubled feeding rate resulted in the same solid material production in the case of spray drying. A rotary atomizer allowed quick solvent evaporation, thanks to the high shear forces, the applied feeding rate was appropriate to make round-shaped SD particles with an average diameter of 13.13 ± 6.25 μm according to the SEM images, and with $d_{(0.5)}$ = 10.766 μm based on the laser diffraction measurement (Figures 3c and 4).

The achieved ~70% yield value of both the methods is satisfactory during the short periods examined as the efficiency may be enhanced with a longer, continuous production process. The main reason for the material losses is that the samples were stuck to the wall of the drying chamber. However, the application of air knives during the process can further increase the yield of the two solvent-based ASD preparation methods. Nonetheless, the equipment used works continuously; therefore, the total productivity could be increased.

3.2. DSC and XRPD Measurements. Examination of the physical state of SPIR in the ES and SD samples was accomplished by DSC and XRPD after drying them for 3 days at room temperature. Pure crystalline SPIR and PVPVA64 were measured as references. The sharp, endothermic melting peak of the crystalline SPIR at 211 °C did not appear in the thermograms of the ES and SD samples, which indicated the amorphous character of the prepared materials (Figure 5a). The wide endothermic sign at the beginning of the thermograms of the ASDs can be explained by the water loss of the polymer.

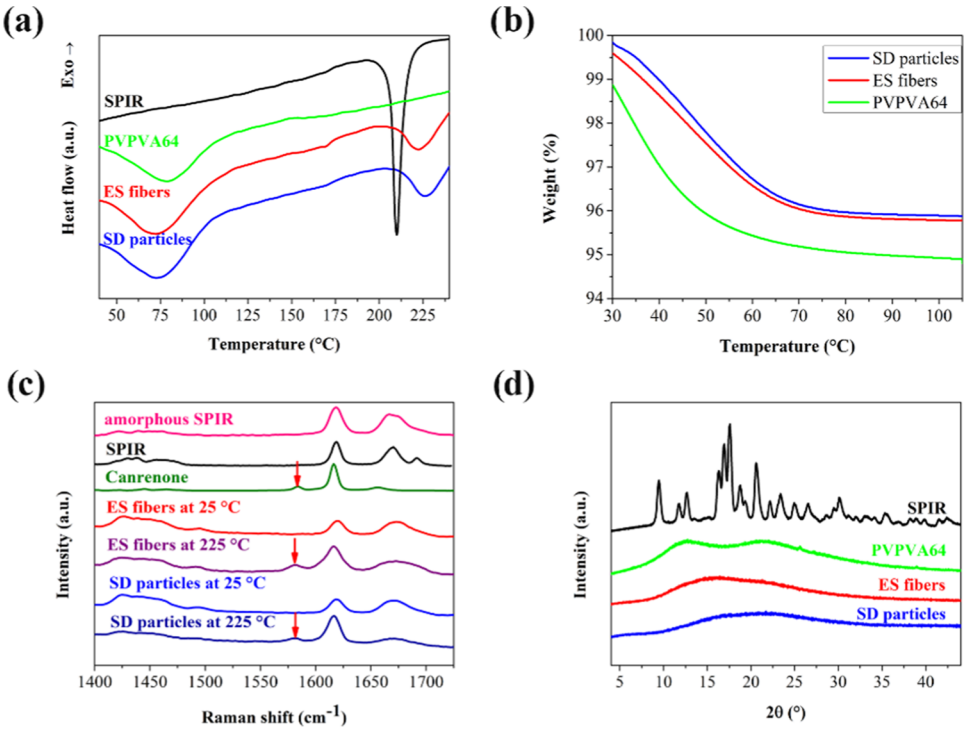

Figure 5. DSC thermograms (a), TGA results (b), Raman spectra (c), and XRPD patterns (d) of the prepared samples. Red arrows on the Raman spectra indicate the characteristic peak of the canrenone.

https://dx.doi.org/10.1021/acs.molpharmaceut.0c00965
Mol. Pharmaceutics 2021, 18, 317−327

Thermogravimetric analysis of the ES and SD samples did not show any significant difference after 3 days of drying at room temperature, and the weight losses were less than that of the pure polymer, which indicated that the ASDs were free of residual solvents after 3 days (Figure 5b). The decomposition of SPIR to canrenone was observed in the thermograms at 223 and 227 °C in the ES and the SD samples, respectively. To differentiate these peaks from the melting peak of the crystalline SPIR, thermogravimetric analysis was performed where the weight loss at the given temperatures showed the decomposition of the API.[50] Furthermore, the characteristic Raman peaks of canrenone (a metabolite of spironolactone) were detectable by Raman spectroscopy, which also proved the decomposition of the API (Figure 5c).[54] XRPD results proved the success of amorphization as well because the sharp peaks of the crystalline SPIR did not appear on the diffractograms of the ES and SD samples (Figure 5d).

3.3. Dissolution Tests. The dissolution results showed a fast release of SPIR from both ASD formulations, which can satisfy the requirements of immediate-release drug products (Figure 6). In addition, standard deviations of the repeated

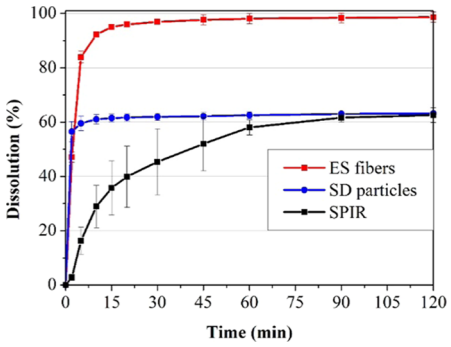

Figure 6. Dissolution profiles of crystalline SPIR, SD particles, and ES fibers. Applied parameters: 37 ± 0.5 °C, 900 mL of 0.1 M HCl dissolution medium, 50 mg of the API content, tapped basket method, 50 rpm, $n = 3$.

measurements proved to be negligible thus, it can be stated that a high macroscopic homogeneity of the powders was reached. However, a lower dissolution extent was observed during the measurements of SD samples. After an initial rapid increase in the dissolution, a plateau was achieved in the first 10 min since very quick precipitation took place in the case of the SD material. The ES fibers dissolved nearly 100%, while the maximal dissolution of the SD particles reached only the value of the micronized crystalline SPIR, which suggested that the SD material recrystallized in the dissolution media.

A comparison of the dissolution media of the ES and SD materials highlighted that the precipitation of the API from the SD particles was clearly visible (Figure 7). The opaque solution indicates that SPIR was in a supersaturated state, and no more API could dissolve in the dissolution media. The dissolution of the prepared ASDs was investigated with a borescope as well. The probe in pure dissolution media showed a black background. At the beginning of the test, the ES fibers dispersed in the dissolution media while the SD particles precipitated almost immediately. Both effects could be tracked with the probe, which showed turbid solutions in the first minute. After 120 min, the ES fibers dissolved completely in 0.1 M HCl medium, and the image of the probe showed the black background again. The precipitation of the SD samples was

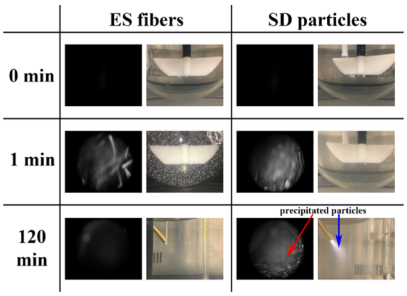

Figure 7. Recordings of the borescope about the dissolution (images with the dark background) and photos about the dissolution media, the paddle, and the probe. The red arrow indicates the precipitated particles, which were visible in the borescope image. The blue arrow indicates light scattering due to the precipitated particles.

observed even at the end of the dissolution tests, where the recordings of the probe indicated the precipitated particles. Based on the results, the applied borescope is a promising tool to monitor the effect of supersaturation and predict the dissolution of quick precipitation systems.

For a better understanding of the dissolution process, Raman spectroscopy was used to monitor the precipitation caused by the dissolution media (Figure 8). A small volume of the HCl

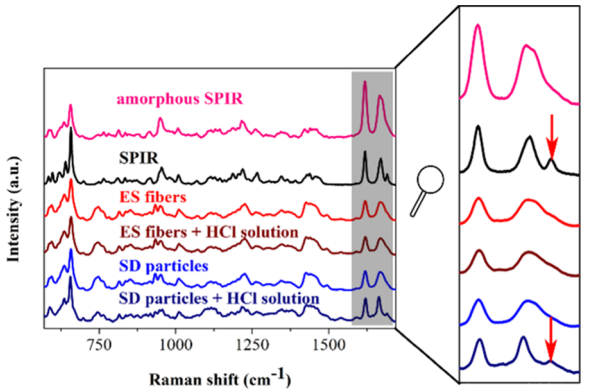

Figure 8. Raman spectra of the ES and SD samples before (ES fibers and SD particles) and after (ES fibers + HCl solution and SD particles + HCl solution) coming in contact with the dissolution media. Red arrow indicates the most characteristic peak of crystalline SPIR.

medium was dropped onto the surface of the ES and SD pastilles to imitate and examine the processes that occur during the dissolution. The Raman spectra of the starting materials show band-broadening, which suggests that SPIR was in the amorphous form within the ASDs.[54] However, narrow peaks appeared in the spectra of SD pastilles after coming in contact with the dissolution media. The most characteristic peak of crystalline SPIR can be seen at 1690 cm^{-1}; therefore, it can be stated that the dissolution media induced quick crystallization of the amorphous SD samples.[55]

3.4. Micro-Morphological Background of Quick Precipitation of SD Samples. According to the DSC, XRPD, and Raman spectroscopy results, the ES and SD samples were amorphous before the dissolution test, and no significant differences were observed between these materials. Based on the measurements, the difference in the dissolution properties of the ASD samples cannot be explained. Although the dissolution tests of the two samples showed remarkable differences, an in-

https://dx.doi.org/10.1021/acs.molpharmaceut.0c00965
Mol. Pharmaceutics 2021, 18, 317−327

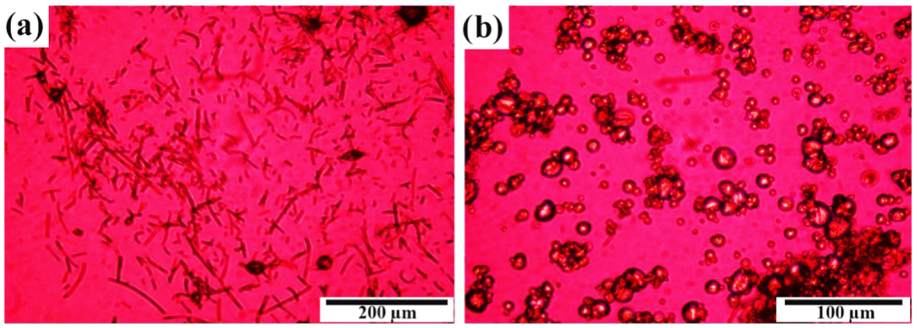

Figure 9. Polarized microscopic images of ES fibers (a) (4× magnification) and SD particles (b) (6.3× magnification).

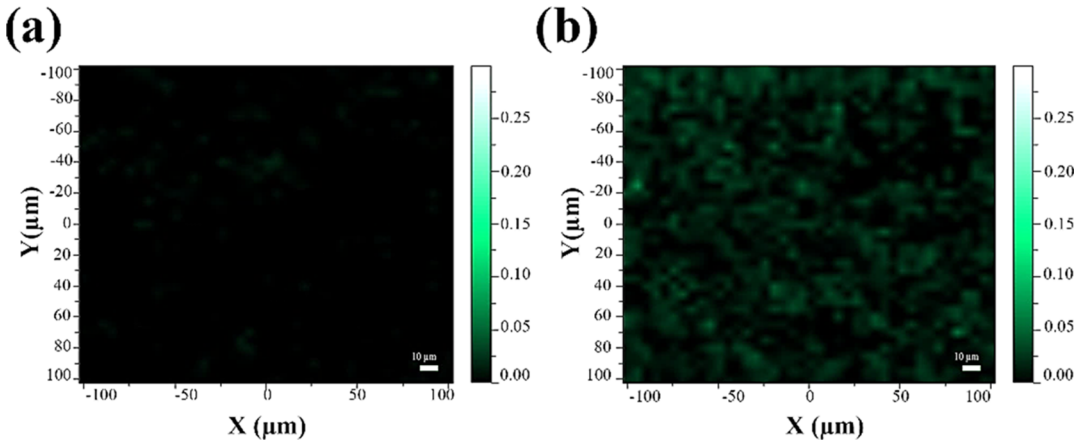

Figure 10. Raman mapping of the ES fibers (a) and the SD particles (b).

depth investigation of the ES fibers and the SD particles was needed.

The polarized light microscopy images did not show birefringence in the ES samples (Figure 9a), while some little green and purple spots were visible in the SD material, which indicated traces of crystallites (Figure 9b). Birefringence was visible almost on every single particle. Although the amount of crystallized samples just reached the limit of detection of polarized light microscopy, the dissolution of SD powder deteriorated significantly. Consequently, crystalline SPIR should be detected using more sensitive analytical methods.[50]

To measure the exact amount of crystalline traces, Raman microscopy mapping was carried out (Figure 10). This analytical tool proved to be appropriate for detecting small quantities of crystalline SPIR with local analysis. In addition, CLS modeling made it possible to determine the crystalline percentage of the samples using crystalline and amorphous SPIR as references. As expected, the SD powder contained plenty of local crystalline traces (Figure 10b), while no noticeable crystallinity was observed in the case of the fibrous samples (Figure 10a). The local quantity of crystalline SPIR at the investigated points reached 5−7% in the SD material. This value was below 1% in the ES samples, which is comparable with the model error of CLS. The existing crystalline nuclei in the SD particles (and the related arrangement of the surrounding randomly arranged molecules) allowed rapid crystallization under the dissolution circumstances and the presence of the solvent accelerated the molecular movement leading to crystal growth. The Raman mapping gave a good explanation for the better dissolution properties of the fibrous material. These results correlated well with our previous results where the relationship between the crystalline traces and dissolution was investigated.[50]

From the polarized microscopic images and the Raman mapping, it can be deduced that the molecular dispersity of the API was not perfect in the SD samples.[56] This unequal molecular dispersity in the ASD led to the formation of crystalline traces, which induced precipitation during dissolution.

3.5. Investigation of the Possible Reasons for the Formation of Crystalline Traces. The dissolution results of the ES and SD samples made clear that the differences in the ASD preparation methods have a huge impact on the physical properties of the generally amorphous product. Consequently, the prepared ASD samples reacted differently in the dissolution media, which was due to the presence of crystalline traces in the SD particles. To explore the origin of the micro-morphological difference, a more detailed analysis was performed.

The solvent evaporation rate can be a possible factor influencing the formation of crystalline traces. Since the drying kinetics during ASD preparation is difficult to determine, the weight loss of the samples at 25 °C was measured right after its preparation. The weight-loss rates of residual solvents in the first 20 min were 0.125 and 0.09 w/w %/min in the case of the ES and SD samples, respectively. It can be stated that the higher specific surface area of ES fibers facilitates solvent evaporation after ASD preparation, which may be similar during solid particle formation. Slower solvent evaporation can result in supersaturated areas for a longer time during the preparation of ASDs, where the API molecules can arrange to form a crystalline structure.

The influence of the evaporation rate on the dissolution was also examined by the preparation of the film-cast (FC) sample (Figure 11). Because solvent evaporation during film casting is relatively slow, the effect of the drying kinetic can be investigated well.[26] The polarized microscopic images of the FC product

https://dx.doi.org/10.1021/acs.molpharmaceut.0c00965
Mol. Pharmaceutics 2021, 18, 317−327

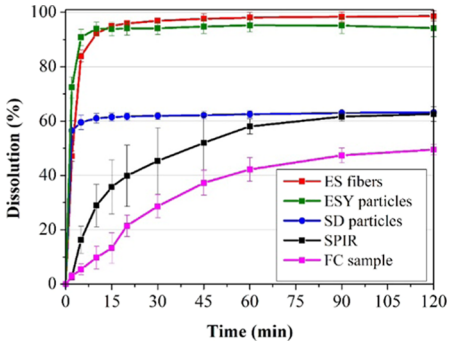

Figure 11. Dissolution profiles of the FC samples, the crystalline SPIR, the SD particles, the ESY particles, and the ES fibers. Applied parameters: 37 ± 0.5 °C, 900 mL of 0.1 M HCl dissolution medium, 50 mg of the API content, tapped basket method, 50 rpm, n = 3.

showed birefringence, which refers to the crystallinity of the sample. The dissolution profile of the FC sample confirmed the formation of crystalline traces because the lower evaporation rate of the residual solvents results in the deterioration of dissolution properties. The lower dissolution of the FC sample compared to the crystalline SPIR may be explained by the larger particle size (Figure 4) and crystallinity of the films.

Besides the evaporation rate of solvents, the electrostatic field might have an influence on particle formation and the drying kinetic during the ASD preparation methods. To identify the effect of the electrostatic forces on the product quality and thus on the dissolution, electrospraying was performed. The application of this electrostatic force-based method resulted in round-shaped particles instead of fibrous structures due to the half concentration of the feed solution. The morphology of the ESY sample showed similarity to the SD particles while the average diameter of the ESY particles was 6.48 ± 3.89 μm according to the SEM images, which is approximately half that of the SD samples (d = 13.13 ± 6.25 μm). The dissolution of the ESY particles proved to be better compared to the SD sample (Figure 11). The results assumed that the formation of local crystalline traces was avoidable in the presence of an electrostatic field since dissolution reached almost the level of the ES fibers. The explanation of these results can be that Coulomb fission during the electrostatic force-based methods affects the evaporation rate and contributes to the orientation of the API molecules in the ASDs.[57−59] Further investigation of electrospraying might be needed for a deeper understanding of the effect of the electrostatic field on particle formation.

4. CONCLUSIONS

Multifunctional equipment was successfully applied to prepare ES fibers and SD particles in a continuous way with similar productivity. Both produced samples proved to be amorphous according to the DSC and XRPD results. The increased specific surface area and the amorphous forms facilitated the dissolution, and thus immediate drug release was realized. However, the dissolution extent enhanced only for the ES product while the SD sample showed a similar final release of crystalline SPIR. In further experiments, the origin of the deterioration of dissolution properties was examined. Traces of crystallinity in the SD particles was detected by polarized microscopy and Raman mapping. The latter was able to determine the local amounts (5−7%) of the crystalline impurity in the SD sample using CLS modeling, which provides the explanation for the precipitation of SD particles during dissolution. According to the findings of this research, electrospinning seemed to be more effective in the context of amorphization of the investigated API-polymer composition. A simple mass loss analysis of ES and SD products showed that the faster solvent evaporation rate during the electrospinning can be a possible reason for the preparation of a more stable amorphous system, which retains its advantageous properties even during the dissolution tests. Furthermore, the preparation of FC and ESY samples revealed that the size and shape of the products, and the electrostatic forces might influence the efficiency of the amorphization in the case of the presented SPIR-PVPVA64 composition.

It is important to note that the evaporation rate of solvents can vary over a wide range during spray drying, which results in either hardly detectable or even easily measurable crystallinity in the product.[60] Consequently, the dissolution of the SD samples depends largely on the process parameter of the preparation method.[48,61] In contrast to spray drying, electrospinning provides a more reliable way to prepare ASDs without crystalline traces since the electrostatic forces contribute to more effective solvent evaporation. Therefore, the preparation method plays a particularly important role in the case of noninteracting ASDs because no intermolecular or intramolecular hydrogen-bonds and interactions can be formed, which could prevent recrystallization during the dissolution or the storage if there are crystalline impurities in the system. In conclusion, electrospinning proved to be a promising and competitive technology with the widely used spray drying to formulate ASDs.

AUTHOR INFORMATION

Corresponding Authors

Guy Van denMooter − *Department of Pharmaceutical and Pharmacological Sciences, Drug Delivery and Disposition, KU Leuven, 3000 Leuven, Belgium*; Phone: +32 16 330 304; Email: guy.vandenmooter@kuleuven.be; Fax: +32 16 330 305

Zsombor K. Nagy − *Department of Organic Chemistry and Technology, Budapest University of Technology and Economics (BME), H-1111 Budapest, Hungary*; orcid.org/0000-0003-2651-7756; Phone: +36 1463-1424; Email: zsknagy@oct.bme.hu; Fax: +36 1463-3648

Authors

Edina Szabó − *Department of Organic Chemistry and Technology, Budapest University of Technology and Economics (BME), H-1111 Budapest, Hungary*

Petra Záhonyi − *Department of Organic Chemistry and Technology, Budapest University of Technology and Economics (BME), H-1111 Budapest, Hungary*

Dániel Brecska − *Department of Organic Chemistry and Technology, Budapest University of Technology and Economics (BME), H-1111 Budapest, Hungary*

Dorián L. Galata − *Department of Organic Chemistry and Technology, Budapest University of Technology and Economics (BME), H-1111 Budapest, Hungary*

Lilla A. Mészáros − *Department of Organic Chemistry and Technology, Budapest University of Technology and Economics (BME), H-1111 Budapest, Hungary*

Lajos Madarász − *Department of Organic Chemistry and Technology, Budapest University of Technology and Economics (BME), H-1111 Budapest, Hungary*

https://dx.doi.org/10.1021/acs.molpharmaceut.0c00965
Mol. Pharmaceutics 2021, 18, 317−327

Kristóf Csorba − *Department of Automation and Applied Informatics, Budapest University of Technology and Economics (BME), H-1111 Budapest, Hungary*
Panna Vass − *Department of Organic Chemistry and Technology, Budapest University of Technology and Economics (BME), H-1111 Budapest, Hungary*
Edit Hirsch − *Department of Organic Chemistry and Technology, Budapest University of Technology and Economics (BME), H-1111 Budapest, Hungary*
Joanna Szafraniec-Szczęsny − *Department of Pharmaceutical Technology and Biopharmaceutics, Faculty of Pharmacy, Jagellonian University Medical College, 30-688 Krakow, Poland*
István Csontos − *Department of Organic Chemistry and Technology, Budapest University of Technology and Economics (BME), H-1111 Budapest, Hungary*
Attila Farkas − *Department of Organic Chemistry and Technology, Budapest University of Technology and Economics (BME), H-1111 Budapest, Hungary*
György Marosi − *Department of Organic Chemistry and Technology, Budapest University of Technology and Economics (BME), H-1111 Budapest, Hungary*

Complete contact information is available at:
https://pubs.acs.org/10.1021/acs.molpharmaceut.0c00965

Author Contributions

The manuscript was written with the contributions of all authors. All authors have approved the final version of the manuscript.

Notes

The authors declare no competing financial interest.

■ ACKNOWLEDGMENTS

This work was performed in the frame of the FIEK_16-1-2016-0007 project, implemented with the support provided by the National Research, Development and Innovation Fund of Hungary, financed under the FIEK_16 funding scheme. This research was supported by grants from the National Research, Development and Innovation Office of Hungary (grant numbers: KH-112644, FK-132133, and PD-121143). Attila Farkas acknowledges the financial support received through the PREMIUM post-doctorate research program of the Hungarian Academy of Sciences. Support of CELSA Research Fund is kindly acknowledged for grant CELSA/19/028. This project was supported by the ÚNKP-20-2-I, the ÚNKP-20-3-I and the ÚNKP-20-4-I New National Excellence Program of the Ministry of Human Capacities. The authors would like to thank Dr. János Madarász for his help with the XRPD experiments. The assistance provided by Erzsébet Tóth with the TGA measurements is also appreciated. The authors would like to express their gratitude to Balázs Pinke for his help with the SEM measurement.

■ REFERENCES

(1) Hertzberg, R. P.; Pope, A. J. High-throughput screening: new technology for the 21st century. *Curr. Opin. Chem. Biol.* **2000**, *4*, 445−451.
(2) Liu, R.; Li, X.; Lam, K. S. Combinatorial chemistry in drug discovery. *Curr. Opin. Chem. Biol.* **2017**, *38*, 117−126.
(3) Vamathevan, J.; Clark, D.; Czodrowski, P.; Dunham, I.; Ferran, E.; Lee, G.; Li, B.; Madabhushi, A.; Shah, P.; Spitzer, M.; Zhao, S. Applications of machine learning in drug discovery and development. *Nat. Rev. Drug Discovery* **2019**, *18*, 463−477.
(4) Lipinski, C. A. Drug-like properties and the causes of poor solubility and poor permeability. *J. Pharmacol. Toxicol. Methods* **2000**, *44*, 235−249.
(5) Fahr, A.; Liu, X. Drug delivery strategies for poorly water-soluble drugs. *Expert Opin. Drug Delivery* **2007**, *4*, 403−416.
(6) Pouton, C. W. Formulation of poorly water-soluble drugs for oral administration: physicochemical and physiological issues and the lipid formulation classification system. *Eur. J. Pharm. Sci.* **2006**, *29*, 278−287.
(7) He, Y.; Ho, C. Amorphous solid dispersions: utilization and challenges in drug discovery and development. *J. Pharm. Sci.* **2015**, *104*, 3237−3258.
(8) Jermain, S. V.; Brough, C.; Williams, R. O., III Amorphous solid dispersions and nanocrystal technologies for poorly water-soluble drug delivery−an update. *Int. J. Pharm.* **2018**, *535*, 379−392.
(9) Vasconcelos, T.; Marques, S.; das Neves, J.; Sarmento, B. Amorphous solid dispersions: Rational selection of a manufacturing process. *Adv. Drug Delivery Rev.* **2016**, *100*, 85−101.
(10) Alshehri, S.; Imam, S. S.; Altamimi, M. A.; Hussain, A.; Shakeel, F.; Elzayat, E.; Mohsin, K.; Ibrahim, M.; Alanazi, F. Enhanced dissolution of luteolin by solid dispersion prepared by different methods: Physicochemical characterization and antioxidant activity. *ACS Omega* **2020**, *5*, 6461−6471.
(11) De Mohac, L. M.; Caruana, R.; Cavallaro, G.; Giammona, G.; Licciardi, M. Spray-Drying, Solvent-Casting and Freeze-Drying Techniques: a Comparative Study on their Suitability for the Enhancement of Drug Dissolution Rates. *Pharm. Res.* **2020**, *37*, No. 57.
(12) Saboo, S.; Mugheirbi, N. A.; Zemlyanov, D. Y.; Kestur, U. S.; Taylor, L. S. Congruent release of drug and polymer: a "sweet spot" in the dissolution of amorphous solid dispersions. *J. Controlled Release* **2019**, *298*, 68−82.
(13) Alshehri, S. M.; Shakeel, F.; Ibrahim, M. A.; Elzayat, E. M.; Altamimi, M.; Mohsin, K.; Almeanazel, O. T.; Alkholief, M.; Alshetaili, A.; Alsulays, B.; et al. Dissolution and bioavailability improvement of bioactive apigenin using solid dispersions prepared by different techniques. *Saudi Pharm. J.* **2019**, *27*, 264−273.
(14) Davis, M. T.; Potter, C. B.; Walker, G. M. Downstream processing of a ternary amorphous solid dispersion: The impacts of spray drying and hot melt extrusion on powder flow, compression and dissolution. *Int. J. Pharm.* **2018**, *544*, 242−253.
(15) Ke, P.; Hasegawa, S.; Al-Obaidi, H.; Buckton, G. Investigation of preparation methods on surface/bulk structural relaxation and glass fragility of amorphous solid dispersions. *Int. J. Pharm.* **2012**, *422*, 170−178.
(16) Trasi, N. S.; Bhujbal, S. V.; Zemlyanov, D. Y.; Zhou, Q.; Taylor, L. S. Physical stability and release properties of lumefantrine amorphous solid dispersion granules prepared by a simple solvent evaporation approach. *Int. J. Pharm.: X* **2020**, *2*, No. 100052.
(17) Patterson, J. E.; James, M. B.; Forster, A. H.; Lancaster, R. W.; Butler, J. M.; Rades, T. The influence of thermal and mechanical preparative techniques on the amorphous state of four poorly soluble compounds. *J. Pharm. Sci.* **2005**, *94*, 1998−2012.
(18) Meng, F.; Trivino, A.; Prasad, D.; Chauhan, H. Investigation and correlation of drug polymer miscibility and molecular interactions by various approaches for the preparation of amorphous solid dispersions. *Eur. J. Pharm. Sci.* **2015**, *71*, 12−24.
(19) Mahmoudi, Z. N.; Upadhye, S. B.; Ferrizzi, D.; Rajabi-Siahboomi, A. R. In vitro characterization of a novel polymeric system for preparation of amorphous solid drug dispersions. *AAPS J.* **2014**, *16*, 685−697.
(20) Singh, A.; Van den Mooter, G. Spray drying formulation of amorphous solid dispersions. *Adv. Drug Delivery Rev.* **2016**, *100*, 27−50.
(21) Paudel, A.; Worku, Z. A.; Meeus, J.; Guns, S.; Van den Mooter, G. Manufacturing of solid dispersions of poorly water soluble drugs by spray drying: formulation and process considerations. *Int. J. Pharm.* **2013**, *453*, 253−284.
(22) Grodowska, K.; Parczewski, A. Organic solvents in the pharmaceutical industry. *Acta Pol. Pharm.* **2010**, *67*, 3−12.
(23) Kennedy, M.; Hu, J.; Gao, P.; Li, L.; Ali-Reynolds, A.; Chal, B.; Gupta, V.; Ma, C.; Mahajan, N.; Akrami, A.; Surapaneni, S. Enhanced

bioavailability of a poorly soluble VR1 antagonist using an amorphous solid dispersion approach: a case study. *Mol. Pharmaceutics* **2008**, *5*, 981−993.
(24) Sawicki, E.; Beijnen, J. H.; Schellens, J. H.; Nuijen, B. Pharmaceutical development of an oral tablet formulation containing a spray dried amorphous solid dispersion of docetaxel or paclitaxel. *Int. J. Pharm.* **2016**, *511*, 765−773.
(25) Li, N.; Cape, J. L.; Mankani, B. R.; Zemlyanov, D. Y.; Shepard, K. B.; Morgen, M. M.; Taylor, L. S. Water-induced phase separation of spray dried amorphous solid dispersions. *Mol. Pharmaceutics* **2020**, *17*, 4004−4017.
(26) Janssens, S.; De Zeure, A.; Paudel, A.; Van Humbeeck, J.; Rombaut, P.; Van den Mooter, G. Influence of preparation methods on solid state supersaturation of amorphous solid dispersions: a case study with itraconazole and eudragit e100. *Pharm. Res.* **2010**, *27*, 775−785.
(27) Sóti, P. L.; Nagy, Z. K.; Serneels, G.; Vajna, B.; Farkas, A.; Van der Gucht, F.; Fekete, P.; Vigh, T.; Wagner, I.; Balogh, A.; et al. Preparation and comparison of spray dried and electrospun bioresorbable drug delivery systems. *Eur. Polym. J.* **2015**, *68*, 671−679.
(28) Surana, R.; Pyne, A.; Suryanarayanan, R. Effect of preparation method on physical properties of amorphous trehalose. *Pharm. Res.* **2004**, *21*, 1167−1176.
(29) Huang, Y.; Dai, W.-G. Fundamental aspects of solid dispersion technology for poorly soluble drugs. *Acta Pharm. Sin. B* **2014**, *4*, 18−25.
(30) Vasanthavada, M.; Tong, W.-Q. T.; Joshi, Y.; Kislalioglu, M. S. Phase behavior of amorphous molecular dispersions II: Role of hydrogen bonding in solid solubility and phase separation kinetics. *Pharm. Res.* **2005**, *22*, 440−448.
(31) Sóti, P. L.; Bocz, K.; Pataki, H.; Eke, Z.; Farkas, A.; Verreck, G.; Kiss, É.; Fekete, P.; Vigh, T.; Wagner, I.; et al. Comparison of spray drying, electroblowing and electrospinning for preparation of Eudragit E and itraconazole solid dispersions. *Int. J. Pharm.* **2015**, *494*, 23−30.
(32) Yu, D.-G.; Li, J.-J.; Williams, G. R.; Zhao, M. Electrospun amorphous solid dispersions of poorly water-soluble drugs: A review. *J. Controlled Release* **2018**, *292*, 91−110.
(33) Balogh, A.; Horváthová, T.; Fülöp, Z.; Loftsson, T.; Harasztos, A. H.; Marosi, G.; Nagy, Z. K. Electroblowing and electrospinning of fibrous diclofenac sodium-cyclodextrin complex-based reconstitution injection. *J. Drug Delivery Sci. Technol.* **2015**, *26*, 28−34.
(34) Cleeton, C.; Keirouz, A.; Chen, X.; Radacsi, N. Electrospun nanofibers for drug delivery and biosensing. *ACS Biomater. Sci. Eng.* **2019**, *5*, 4183−4205.
(35) Ambrus, R.; Alshweiat, A.; Csóka, I.; Ovari, G.; Esmail, A.; Radacsi, N. 3D-printed electrospinning setup for the preparation of loratadine nanofibers with enhanced physicochemical properties. *Int. J. Pharm.* **2019**, *567*, No. 118455.
(36) Yang, Y.; Zhu, T.; Liu, Z.; Luo, M.; Yu, D.-G.; Bligh, S. A. The key role of straight fluid jet in predicting the drug dissolution from electrospun nanofibers. *Int. J. Pharm.* **2019**, *569*, No. 118634.
(37) Sun, R.; Shen, C.; Shafique, S.; Mustapha, O.; Hussain, T.; Khan, I. U.; Mehmood, Y.; Anwer, K.; Shahzad, Y.; Yousaf, A. M. Electrosprayed Polymeric Nanospheres for Enhanced Solubility, Dissolution Rate, Oral Bioavailability and Antihyperlipidemic Activity of Bezafibrate. *Int. J. Nanomed.* **2020**, *15*, 705.
(38) Smeets, A.; Koekoekx, R.; Clasen, C.; Van den Mooter, G. Amorphous solid dispersions of darunavir: Comparison between spray drying and electrospraying. *Eur. J. Pharm. Biopharm.* **2018**, *130*, 96−107.
(39) Pérez-Masiá, R.; Lagaron, J. M.; Lopez-Rubio, A. Morphology and stability of edible lycopene-containing micro-and nanocapsules produced through electrospraying and spray drying. *Food Bioprocess Technol.* **2015**, *8*, 459−470.
(40) Kadir, M. F.; Alam, M. R.; Rahman, A. B.; Jhanker, Y. M.; Shams, T.; Khan, R. I. Study of binary and ternary solid dispersion of spironolactone prepared by co-precipitation method for the enhancement of Oral bioavailability. *J. Appl. Pharm. Sci.* **2012**, *2*, 117.
(41) Shamsuddin, M. F.; Ansari, S. H.; Ali, J. Development and evaluation of solid dispersion of spironolactone using fusion method. *Int. J. Pharm. Invest.* **2016**, *6*, 63.
(42) Yassin, A. E. B.; Alanazi, F. K.; El-Badry, M.; Alsarra, I. A.; Barakat, N. S.; Alanazi, F. K. Preparation and characterization of spironolactone-loaded gelucire microparticles using spray-drying technique. *Drug Dev. Ind. Pharm.* **2009**, *35*, 297−304.
(43) Chiu, Y.-J.; Zhang, Z.; Dziemidowicz, K.; Nikoletopoulos, C.-G.; Angkawinitwong, U.; Chen, J.-T.; Williams, G. R. The effect of solvent vapor annealing on drug-loaded electrospun polymer fibers. *Pharmaceutics* **2020**, *12*, 139.
(44) Al-Zoubi, N.; Odah, F.; Obeidat, W.; Al-Jaberi, A.; Partheniadis, I.; Nikolakakis, I. Evaluation of spironolactone solid dispersions prepared by co-spray drying with soluplus and polyvinylpyrrolidone and influence of tableting on drug release. *J. Pharm. Sci.* **2018**, *107*, 2385−2398.
(45) Shah, S.; Joshi, S.; Lin, S.; Madan, P. Preparation and characterization of spironolactone solid dispersions using hydrophilic carriers. *Asian J. Pharm. Sci.* **2012**, *7*, 40−49.
(46) Islam, S. A.; Paul, P. K.; Shahriar, M.; Dewan, I.; Dey, L. R. Comparative in vitro dissolution study of spironolactone from binary and tertiary solid dispersion: model dependant and independent approaches. *J. Drug Delivery Ther.* **2012**, *2* (4), 73−80.
(47) Balogh, A.; Farkas, B.; Domokos, A.; Farkas, A.; Démuth, B.; Borbás, E.; Nagy, B.; Marosi, G.; Nagy, Z. K. Controlled-release solid dispersions of Eudragit FS 100 and poorly soluble spironolactone prepared by electrospinning and melt extrusion. *Eur. Polym. J.* **2017**, *95*, 406−417.
(48) Nagy, Z. K.; Balogh, A.; Démuth, B.; Pataki, H.; Vigh, T.; Szabó, B.; Molnár, K.; Schmidt, B. T.; Horák, P.; Marosi, G.; et al. High speed electrospinning for scaled-up production of amorphous solid dispersion of itraconazole. *Int. J. Pharm.* **2015**, *480*, 137−142.
(49) Vass, P.; Démuth, B.; Farkas, A.; Hirsch, E.; Szabó, E.; Nagy, B.; Andersen, S. K.; Vigh, T.; Verreck, G.; Csontos, I.; et al. Continuous alternative to freeze drying: Manufacturing of cyclodextrin-based reconstitution powder from aqueous solution using scaled-up electrospinning. *J. Controlled Release* **2019**, *298*, 120−127.
(50) Szabó, E.; Démuth, B.; Nagy, B.; Molnár, K.; Farkas, A.; Szabó, B.; Balogh, A.; Hirsch, E.; Marosi, G.; Nagy, Z.; et al. Scaled-up preparation of drug-loaded electrospun polymer fibres and investigation of their continuous processing to tablet form. *eXPRESS Polym. Lett.* **2018**, *12*, 436−451.
(51) Balogh, A.; Farkas, B.; Faragó, K.; Farkas, A.; Wagner, I.; Verreck, G.; Nagy, Z. K.; Marosi, G.; et al. Melt-blown and electrospun drug-loaded polymer fiber mats for dissolution enhancement: a comparative study. *J. Pharm. Sci.* **2015**, *104*, 1767−1776.
(52) Hirsch, E.; Vass, P.; Démuth, B.; Pethő, Z.; Bitay, E.; Andersen, S.; Vigh, T.; Verreck, G.; Molnár, K.; Nagy, Z. K.; et al. Electrospinning scale-up and formulation development of PVA nanofibers aiming oral delivery of biopharmaceuticals. *eXPRESS Polym. Lett.* **2019**, *13*, 590−603.
(53) Vass, P.; Szabó, E.; Domokos, A.; Hirsch, E.; Galata, D.; Farkas, B.; Démuth, B.; Andersen, S. K.; Vigh, T.; Verreck, G. Scale-up of electrospinning technology: Applications in the pharmaceutical industry. *Wiley Interdiscip.Nanomed. Nanobiotechnol.* **2019**, *12*, No. e1611.
(54) Vigh, T.; Drávavölgyi, G.; Sóti, P. L.; Pataki, H.; Igricz, T.; Wagner, I.; Vajna, B.; Madarász, J.; Marosi, G.; Nagy, Z. K. Predicting final product properties of melt extruded solid dispersions from process parameters using Raman spectrometry. *J. Pharm. Biomed. Anal.* **2014**, *98*, 166−177.
(55) Nagy, Z. K.; Balogh, A.; Vajna, B.; Farkas, A.; Patyi, G.; Kramarics, Á.; Marosi, G. Comparison of electrospun and extruded Soluplus-based solid dosage forms of improved dissolution. *J. Pharm. Sci.* **2012**, *101*, 322−332.
(56) Baghel, S.; Cathcart, H.; O'Reilly, N. J. Polymeric amorphous solid dispersions: a review of amorphization, crystallization, stabilization, solid-state characterization, and aqueous solubilization of biopharmaceutical classification system class II drugs. *J. Pharm. Sci.* **2016**, *105*, 2527−2544.

https://dx.doi.org/10.1021/acs.molpharmaceut.0c00965
Mol. Pharmaceutics 2021, 18, 317−327

(57) Almería, B.; Deng, W.; Fahmy, T. M.; Gomez, A. Controlling the morphology of electrospray-generated PLGA microparticles for drug delivery. *J. Colloid Interface Sci.* **2010**, *343*, 125−133.
(58) Mehta, N. A.; Levin, D. A. Electrospray molecular dynamics simulations using an octree-based Coulomb interaction method. *Phys. Rev. E* **2019**, *99*, No. 033302.
(59) Liu, Z.-P.; Zhang, L.-L.; Yang, Y.-Y.; Wu, D.; Jiang, G.; Yu, D.-G. Preparing composite nanoparticles for immediate drug release by modifying electrohydrodynamic interfaces during electrospraying. *Powder Technol.* **2018**, *327*, 179−187.
(60) Savolainen, M.; Heinz, A.; Strachan, C.; Gordon, K. C.; Yliruusi, J.; Rades, T.; Sandler, N. Screening for differences in the amorphous state of indomethacin using multivariate visualization. *Eur. J. Pharm. Sci.* **2007**, *30*, 113−123.
(61) Kim, S.; Gupta, B.; Moon, C.; Oh, E.; Jeong, J.-H.; Yong, C. S.; Kim, J. O. Employing an optimized spray-drying process to produce ezetimibe tablets with an improved dissolution profile. *J. Pharm. Invest.* **2016**, *46*, 583−592.

https://dx.doi.org/10.1021/acs.molpharmaceut.0c00965
Mol. Pharmaceutics 2021, 18, 317−327